Magnons in spin glasses: The high-field limit

I. Avgin and D. L. Huber
Department of Physics, University of Wisconsin–Madison, Madison, Wisconsin 53706

W. Y. Ching
Department of Physics, University of Missouri–Kansas City, Kansas City, Missouri 64110

(Received 16 January 1992)

A study is made of the high-field behavior of the linearized magnetic excitations (magnons) in spin glasses. A $\pm J$ Heisenberg spin Hamiltonian is postulated, and the applied magnetic field is assumed to be sufficiently strong to ensure alignment of the ground state. Numerical calculations of the density of states, the localization indices, and the zero-temperature dynamic structure factor are carried out for a simple-cubic lattice with nearest-neighbor interactions and the results compared with the predictions of a self-consistent theory based on a coherent-exchange approximation. A comparison is also made with the corresponding results obtained in zero applied field.

I. INTRODUCTION

Determining the nature of the ground state and the low-lying excitations in spin glasses continues to be a challenging problem. The high degeneracy of the ground state in zero field precludes standard theoretical treatments analogous to those developed for systems with long-range ferromagnetic or antiferromagnetic order. Despite considerable effort on the part of many investigators, there has yet to emerge a satisfactory microscopic theory that is applicable to the broad class of materials showing spin glass behavior.

The purpose of this paper is to present the results of a study of the excitations in a model spin glass in the high-field limit. By taking the field large enough to ensure (virtually) complete alignment of the ground state, one has a system intermediate in complexity between the spin glass in zero field and the ideal ferromagnet. A study of the high-field excitations in spin glasses has been carried out by Shender.[1] He utilized the connection between the spin wave stiffness and the conductivity of an equivalent network, and an effective-medium theory for the latter, to predict the variation of the stiffness with the degree of disorder in two- and three-dimensional lattices. In this paper, the analysis of Shender is extended in two ways. First, numerical techniques are used to calculate the magnon density of states, the localization indices for the magnon modes, and the zero-temperature dynamic structure factor. Second, the results obtained from the simulation studies are compared with the predictions of a theory based on a coherent-exchange approximation, which reduces to the effective-medium theory of Ref. 1 in an appropriate limit.

The calculations are carried out for the $\pm J$ model of a Heisenberg spin glass,[2] where the Hamiltonian is written

$$\mathcal{H}=-H\sum_j S_j^z-\sum_{(i,j)}{}'J_{ij}\mathbf{S}_i\cdot\mathbf{S}_j \ . \tag{1}$$

Here H is the applied field (in units of $g\mu_B$), and the prime signifies that the summation is limited to nearest-neighbor pairs. The exchange interaction J_{ij} takes on the values J (>0) with probability $1-c$ and the value $-J$ with probability c, there being no correlation between different bonds. (Note that with this choice of sign, $c=0$ describes the ideal ferromagnet.) Detailed results are presented for the simple cubic lattice. Corresponding results for one- and two-dimensional arrays will be presented elsewhere.

When $H\gg J$, the ground state of (1) is effectively one of complete alignment, i.e., $\langle S^z\rangle=S$, S being the magnitude of the spin. In this limit, the linearized equation of motion for the operator S^+ ($=S^x+iS^y$) has the form ($\hbar=1$)

$$i\,dS_j^+/dt=HS_j^+ +S\sum_k{}'J_{jk}(S_j^+-S_k^+) \ . \tag{2}$$

Equation (2), together with the aforementioned distribution for J_{ij},

$$P(J_{ij})=(1-c)\delta(J_{ij}-J)+c\,\delta(J_{ij}+J) \ , \tag{3}$$

forms the basis for the analysis in the rest of the paper. With the assumption of a harmonic time dependence $S^+\sim\exp(-i\omega t)$ one obtains the set of linear equations

$$(\omega-H)a_j=S\sum_k{}'J_{jk}(a_j-a_k) \ , \tag{4}$$

where the Holstein-Primakoff transformation has been used to replace S_j^+ with the boson annihilation operator a_j. The eigenvectors of (4) characterize the spatial properties of the linear magnetic excitations or magnons, whereas the corresponding eigenvalues are the magnon energies.

Two global quantities of interest are obtained from solving Eq. (4): the distribution of eigenvalues, or the magnon density of states, and the localization indices, which are sometimes referred to as the inverse participation ratios. The latter are defined in terms of the eigen-

 ©1992 The American Physical Society

vectors ϕ_j^ν, ν designating the eigenstate, by means of equation[3]

$$L_\nu = \sum_j (\phi_j^\nu)^4 / \left[\sum_j (\phi_j^\nu)^2 \right]^2 . \tag{5}$$

For finite arrays of N spins, $L_\nu \sim N^{-1}$ for extended states, whereas for localized states L_ν^{-1} is a measure of the number of sites on which the mode has significant amplitude.

The zero-temperature dynamic structure factor, which is denoted by $S(\mathbf{Q},E)$, is another measure of the effect of disorder on the spin dynamics. Although $S(\mathbf{Q},E)$ can be expressed in terms of the eigenvectors and eigenvalues, a more direct approach, which avoids diagonalization and thus is applicable to larger arrays of spins, is to work with correlation functions $G_j(\mathbf{Q},t)$ which are defined by [4-6]

$$G_j(\mathbf{Q},t) = \sum_k \langle 0 | a_j(t) a_k^\dagger | 0 \rangle \exp(-i\mathbf{Q}\cdot\mathbf{r}_k) , \tag{6}$$

where $|0\rangle$ is the vacuum state, $\mathbf{Q}$ denotes a vector in the Brillouin zone of the lattice of spins, and $\mathbf{r}_k$ designates the position of the kth spin. The G_j have the equation of motion

$$i\, dG_j(\mathbf{Q},t)/dt = HG_j(\mathbf{Q},t) + \sum_k{}' J_{jk} [G_j(\mathbf{Q},t) - G_k(\mathbf{Q},t)] \tag{7}$$

with the initial condition $G_j(\mathbf{Q},0+) = \exp(-i\mathbf{Q}\cdot\mathbf{r}_j)$. The structure factor is then given by an expression of the form[6]

$$S(\mathbf{Q},E) = -2/(N\pi) \int_0^\infty \sin(Et)\, \mathrm{Im} \left[\sum_j \exp(i\mathbf{Q}\cdot\mathbf{r}_j) \times G_j(\mathbf{Q},t) \right] dt , \tag{8}$$

where Im denotes imaginary part. In applying the method, one integrates the equations of motion and then calculates the structure factor from Eq. (8). In practice, an exponential cutoff factor $\exp(-\alpha t)$ is introduced in the integrand, and the integral is evaluated to a time T where $\alpha T \gg 1$. For Lorentzian line shapes, the cutoff factor is equivalent to an "instrumental" width equal to α.

II. NUMERICAL RESULTS

In this section, results are presented for the magnon density of states, the localization indices, and the zero-temperature dynamic structure factor for the simple cubic lattice in the high-field limit. The systems are characterized by the Hamiltonian (1) with the nearest-neighbor interactions having the distribution given in Eq. (3). In all cases $J=S=1$, so that the width of the magnon band when $c=0$ is equal to 12. Results are reported for $c=0.05$, 0.10, 0.20, 0.30, 0.40, and 0.50. (The results for $c>0.5$ are obtained from those with $c<0.5$, by reflecting about the point $E-H=0$.)

Figure 1 is a histogram showing the distribution of the magnon energies. For each value of c, the data are from five configurations of an $8\times8\times8$ array with periodic boundary conditions. Particularly noteworthy is the shift in the distribution to lower energies with increasing c. When $c=0$, the lower edge of the magnon band is at the

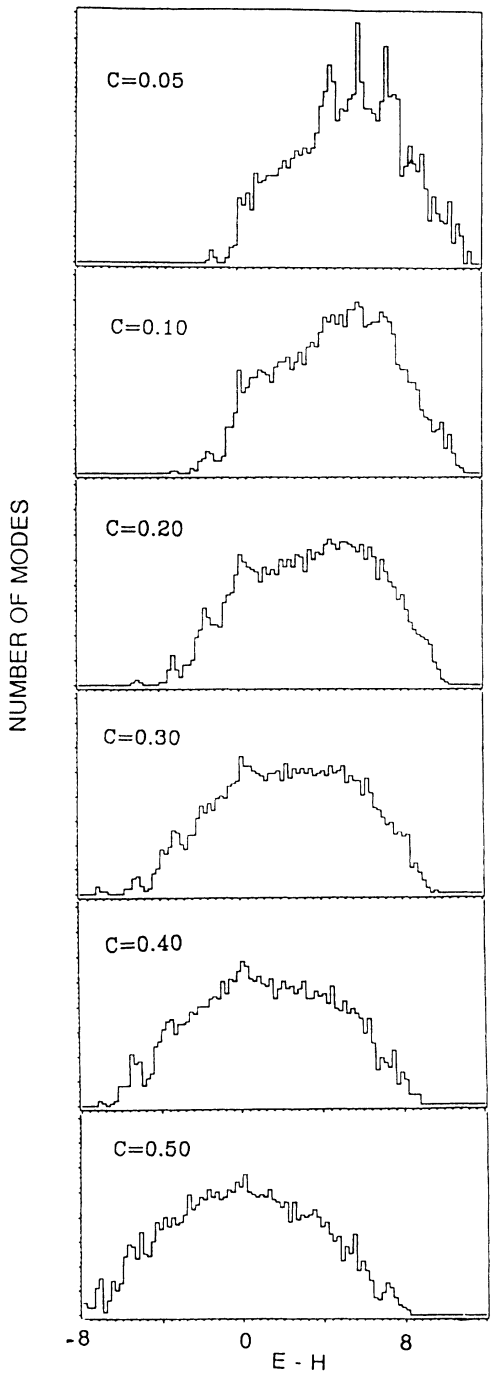

FIG. 1. Distribution of magnon energies for various values of c. Data are from five configurations of an $8\times8\times8$ array. $J=S=1$. The vertical scale is between 0 and 80, except for $c=0.05$, where the range is between 0 and 100. In this and subsequent figures E denotes the energy and H is the magnetic field in units of $g\mu_B$.

point $E=H$; when $c=1$, the *upper* edge of the band is at $E=H$, and when $c=0.50$, the band is distributed symmetrically (in the thermodynamic limit) about $E=H$, extending from $E=H-8$ to $H+8$.

Figure 2 shows the distribution of localization indices for single configurations of $8\times8\times8$ arrays. For $c=0.05$ almost all modes are (quasi)delocalized; localized modes are present only at the bottom of the band. With increasing disorder, localized modes appear also at the top of the band, until at $c=0.50$, they are (approximately) uniformly distributed about the point $E=H$.

Figure 3 shows the results for the zero-temperature dy-

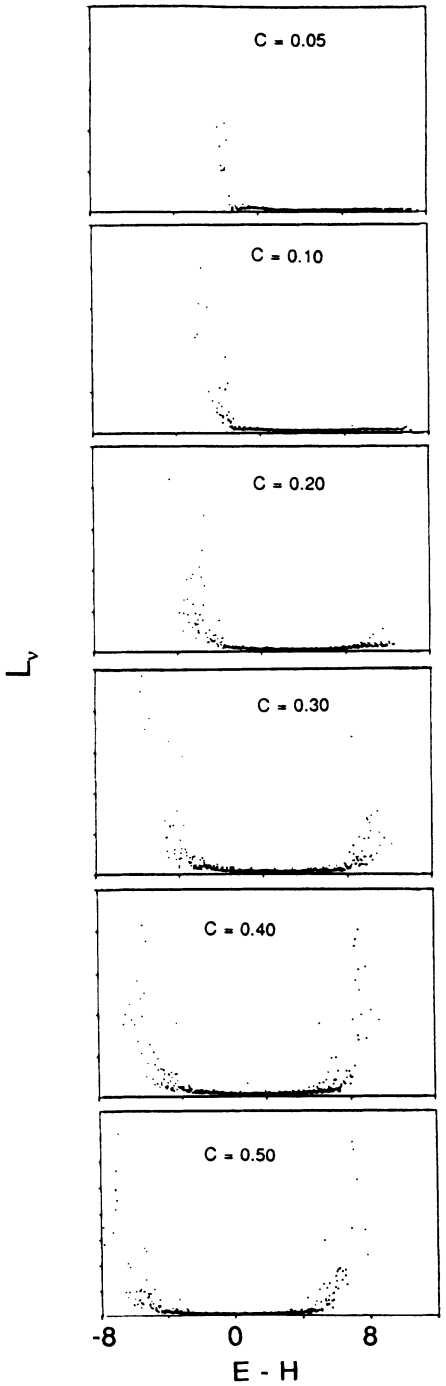

FIG. 2. Localization indices L_ν for various values of c. Data are from a single configuration of an $8\times8\times8$ array. Similar results are obtained with other configurations. $J=S=1$. The vertical scale is between 0 and 0.25, except for $c=0.50$, where the range is between 0 and 0.40.

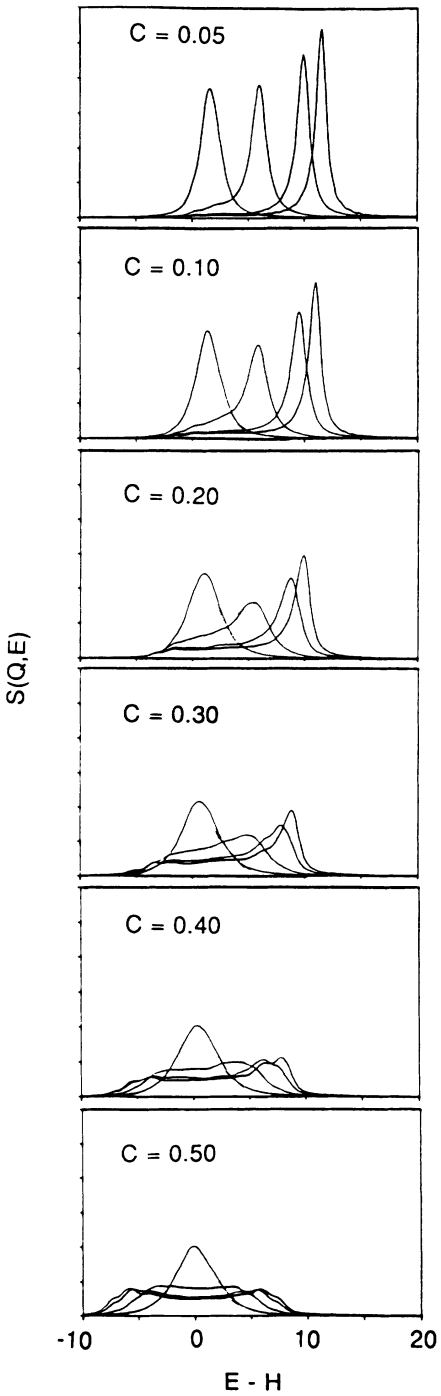

FIG. 3. Zero-temperature dynamic structure factor for various values of c. Viewed from right to left, the four curves correspond to $\mathbf{Q}=(\pi/8)(n,n,n)$ with $n=8$, 6, 4, and 2. Data are from a single configuration of a $16\times16\times16$ array. All curves have the same area and are calculated from Eq. (7) with the cutoff factor $\exp(-0.5t)$. $J=S=1$. In all panels, the vertical scale is between 0 and 0.6.

namic structure factor. The data were obtained from single configurations of $16\times16\times16$ arrays. The curves were calculated using Eq. (8) with $\alpha=0.5$ in the exponential cutoff factor. From right to left, the curves are associated with the wave vectors $\mathbf{Q}=(\pi/8)(n,n,n)$ with $n=8$, 6, 4, and 2. With increasing disorder, the peaks in the dynamic structure factor broaden and shift to lower energy. A tail develops on the low-energy side which evolves into a satellite peak. At $c=0.50$, the structure factors associated with the larger values of $\mathbf{Q}$ ($n=4$, 6, and 8) show significant spectral weight over the range $-8<E-H<8$, whereas the structure factor for the smallest $\mathbf{Q}$ ($n=2$) is peaked at $E=H$. This behavior is an example of a "kinematic effect." Since the total spin $\sum\mathbf{S}_j$ commutes with the Heisenberg exchange interaction, the zero-temperature dynamic structure factor associated with the center of the zone $S(\mathbf{0},E)$ consists of a δ function centered a the point $E=H$. For $\mathbf{Q}\approx\mathbf{0}$, the δ function becomes a narrow peak.

III. COHERENT-EXCHANGE APPROXIMATION

This section is devoted to a presentation of the results for the magnon density of states and the zero-temperature dynamic structure factor that are obtained using a coherent-exchange approximation. The coherent-exchange approximation, which is a variation of the coherent-potential approximation for random alloys, was used by Tahir-Kheli in his treatment of dilute ferromagnets and antiferromagnets.[7] In this approximation, the configurational average of the zero-temperature Green's function is written

$$\langle G(E-H,\mathbf{Q})\rangle=[E-H-J_c(E-H)Sz(1-\gamma_{\mathbf{Q}})]^{-1}\ , \tag{9}$$

where z is the number of nearest neighbors (interactions are assumed to be only between nearest neighbors) and γ_Q has the form

$$\gamma=z^{-1}\sum_k{}'\exp[i\mathbf{Q}\cdot(\mathbf{r}_j-\mathbf{r}_k)]\ , \tag{10}$$

in which the sum on k is over the z nearest neighbors of the site j.

The coherent-exchange integral $J_c(E-H)$ is obtained as a solution to the self-consistent equation

$$\int djP(j)(j-J_c)/[1-2(j-J_c)Sf(E-H)]=0\ , \tag{11}$$

where $P(j)$ denotes the distribution of nearest-neighbor interactions and

$$f(E-H)=\langle G_0(E-H)\rangle-\langle G_1(E-H)\rangle\ , \tag{12}$$

with

$$\langle G_0(E-H)\rangle=N^{-1}\sum_{\mathbf{Q}}\langle G(E-H,\mathbf{Q})\rangle \tag{13}$$

and

$$\begin{aligned}\langle G_1(E-H)\rangle&=N^{-1}\sum_{\mathbf{Q}}\gamma_Q\langle G(E-H,\mathbf{Q})\rangle\\&=\langle G_0(E-H)\rangle\\&\quad-[(E-H)\langle G_0(E-H)\rangle-1]/J_cSz\ .\end{aligned} \tag{14}$$

In the limit $E\to H$, which is relevant for the characterization of the long-wavelength excitations (i.e., those with $\mathbf{Q}\approx\mathbf{0}$), one has $f(0)=-1/J_cSz$ so that Eq. (11) becomes

$$\int dj\,P(j)(j-J_c)[J_c(z/2-1)+j]^{-1}=0\ , \tag{15}$$

which is equivalent to the effective-medium approximation of Ref. 1.

Having obtained J_c from the solution to Eq. (11), the density of states $\rho(E)$ and the zero-temperature dynamic structure factor are given by[7]

$$\rho(E)=-(1/\pi)\,\mathrm{Im}\langle G_0(E-H+i\varepsilon)\rangle \tag{16}$$

and

$$S(\mathbf{Q},E)=-(1/\pi)\,\mathrm{Im}\langle G(E-H+i\varepsilon,\mathbf{Q})\rangle\ , \tag{17}$$

respectively.

The calculation of the density of states and the dynamic structure factor entails solving Eq. (11) for $J_c(E-H)$ using the distribution displayed in Eq. (3). In carrying out the numerical analysis, it has proven convenient to use an approximate expression for the Green's function. In the case of no disorder, $\langle G_0\rangle$ has the form

$$\begin{aligned}\langle G_0(E-H)\rangle=(8/M)(E-H-0.5\\-\{[(E-H)/M]^2\\-(E-H)/M\}^{1/2})\ ,\end{aligned} \tag{18}$$

where the magnon bandwidth M is equal to $12JS(c=0)$. Equation (18), which has been used by Hubbard,[8] is equivalent to approximating the density of states of a simple-cubic array by a semicircle. In using (18) in the coherent-exchange approximation, M is replaced by $12J_cS$.

Although (18) introduces some error into the results, particularly at small c, it has the virtue of being a simple analytic approximation. The alternative, which is to evaluate $\langle G_0\rangle$ using Eq. (13), involves integration over a three-dimensional Brillouin zone at each step in achieving self-consistency, which in itself introduces error and greatly adds to the complexity of the analysis.

The results for the density of states and the dynamic

structure factor that are obtained with the coherent-exchange approximation are shown in Figs. 4 and 5, respectively. All curves were calculated with $\mathrm{Im}E=0.5$, which corresponds to the cutoff factor $\exp(-0.5t)$ that was used in the numerical evaluation of $S(\mathbf{Q},E)$ discussed in Sec. II. As will be discussed in detail in the next section, there is qualitative and, in some instances, quantitative agreement between the simulation data and the predictions of the coherent-exchange approximation.

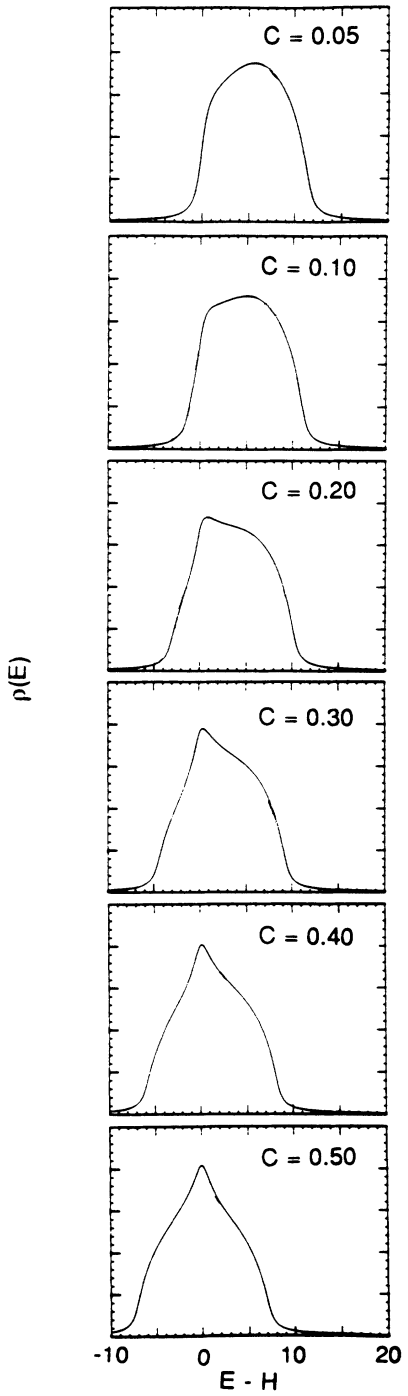

FIG. 4. Magnon density of states according to the coherent-exchange approximation for various values of c. All curves have the same area and are calculated from Eq. (16) with $\varepsilon=0.5$ and $J=S=1$. The curves are to be compared with the corresponding data displayed in Fig. 1. In all panels, the vertical scale is between 0 and 0.125.

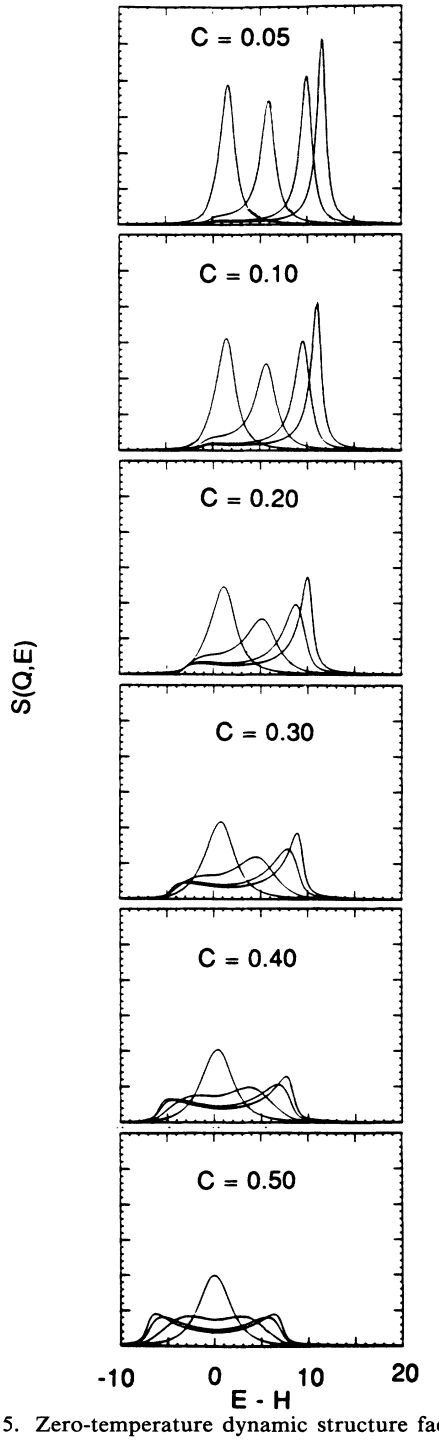

FIG. 5. Zero-temperature dynamic structure factor according to the coherent-exchange approximation for various values of c. Viewed from right to left, the four curves correspond to $\mathbf{Q}=(\pi/8)(n,n,n)$ with $n=8$, 6, 4, and 2. All curves have the same area and are calculated from Eq. (17) with $\varepsilon=0.5$ and $J=S=1$. The curves are to be compared with the corresponding curves displayed in Fig. 3. In all panels the vertical scale is between 0 and 0.6.

IV. DISCUSSION

As noted, there is good qualitative agreement between the predictions of the coherent-exchange approximation and the numerical data. The coherent exchange approximation accounts reasonably well for the changes in the density of states, including the shifts in the upper and lower band edges with increasing disorder. The agreement between the theory and simulation is particularly impressive for the dynamic structure factor, extending even to $c=0.50$, where the disorder is at a maximum.

A particularly interesting feature of the figure displaying the localization indices (Fig. 2) is the appearance of localized modes in the neighborhood of $E-H=0$ for c as small as 0.05. Such a result is predicted by the coherent-exchange approximation in the effective-medium limit. With the distribution given by Eq. (3), Eq. (11) yields the solution[1]

$$J_c(E-H=0)/J=\{3(1-2c)+[9(1-2c)^2-8]^{1/2}\}/4\ , \tag{19}$$

for $z=6$, and $0\le c\le 0.50$. For $c>\frac{1}{2}-2^{1/2}/3=0.029\ldots$, $J_c(0)$ is complex, becoming equal to $i/2^{1/2}J$ when $c=0.50$. The presence of an imaginary part in $J_c(0)$ is connected with the appearance of localized modes in the neighborhood of $E-H=0$.[1] With larger c the long-wavelength modes become increasingly damped. At $c=0.50$ the modes are entirely overdamped with the spectral weight centered at $E-H=0$. Note that the behavior of J_c when $E-H=0$ contrasts with the corresponding behavior when $|E-H|\gg J$. In this limit, J_c is equal to the mean value of the exchange interaction $\int dj\, P(j)j$ which is $(1-2c)J$ for the $\pm J$ model.

In Figs. 6, 7, and 8, data are presented for the density of states, the localization indices, and the zero-temperature dynamic structure factor in zero field over the same parameter ranges as in Figs. 1–3. The calculations were carried out with ground-state configurations obtained by the method of simulated quenching described in Refs. 3 and 6. Noticeable in Fig. 6 is the shift in the eigenvalue distribution to lower energy with increasing disorder. Figure 7 shows the corresponding behavior of the localization indices. Surprisingly, for weak disorder $c<0.30$ the modes near zero are the more localized, whereas for strong disorder $c\ge 0.30$ the localized modes are at the top of the band.

The behavior of the dynamic structure factor shown in Fig. 8 reveals that the magnon peaks broaden and shift to lower energies with increasing disorder. For $c\ge 0.20$, the peaks are significantly distorted with low-energy tails. The apparent peaks at $E\approx 0$ for $\mathbf{Q}=(\pi/8)(1,1,1)$ are an artifact of the simulation method which forces $S(\mathbf{Q},0)$ to be zero, with the falloff occurring over an interval equal to α, the parameter in the cutoff factor in Eq. (8).[6,9] Because of this it is concluded that for $c\ge 0.3$, the low-frequency modes are delocalized but nonpropagating whereas the high-frequency modes are strongly localized.

To summarize, the most significant result to emerge from this study is the finding that the coherent-exchange approximation gives a good account of the distribution of magnon modes and the zero-temperature dynamic structure factor of a spin glass in the high-field limit. Although the results were obtained for the $\pm J$ model, one expects equal success for other distributions of nearest-neighbor exchange integrals (e.g., Gaussian). It should be noted that the use of the coherent-exchange approxima-

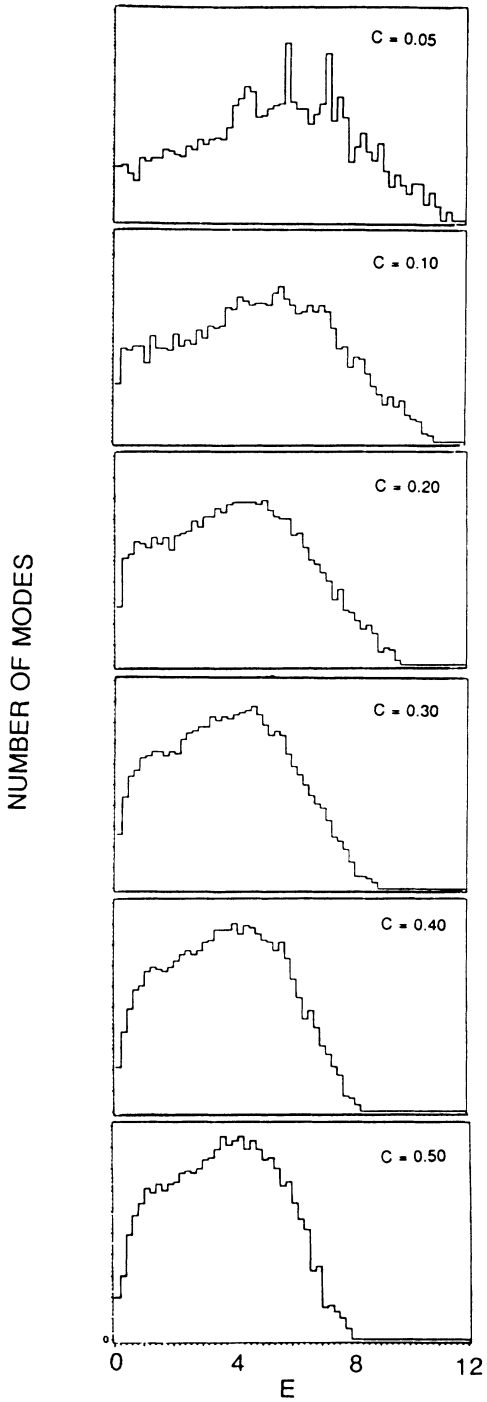

FIG. 6. Distribution of magnon modes in zero field for various values of c. Other parameters the same as in Fig. 1. The vertical scale is between 0 and 100, except for $c=0.05$, where the range is between 0 and 120.

tion requires a ferromagnetic (or antiferromagnetic) ground state. Thus, it cannot be applied to the spin glass in zero field. It remains a challenge to develop an equivalent theory fro the zero-field excitations in Heisenberg spin glasses. Finally, it should be stressed that care should be taken in applying the coherent-exchange theory to real materials. The approach assumes no correlation between different bonds, whereas in most spin glasses, e.g., $Eu_{1-x}Sr_xS$, a disorder is introduced by a random doping of impurities, leading to random site disorder as opposed to random bond disorder. For such systems, the predictions of the theory can only be expected to be qualitatively correct.

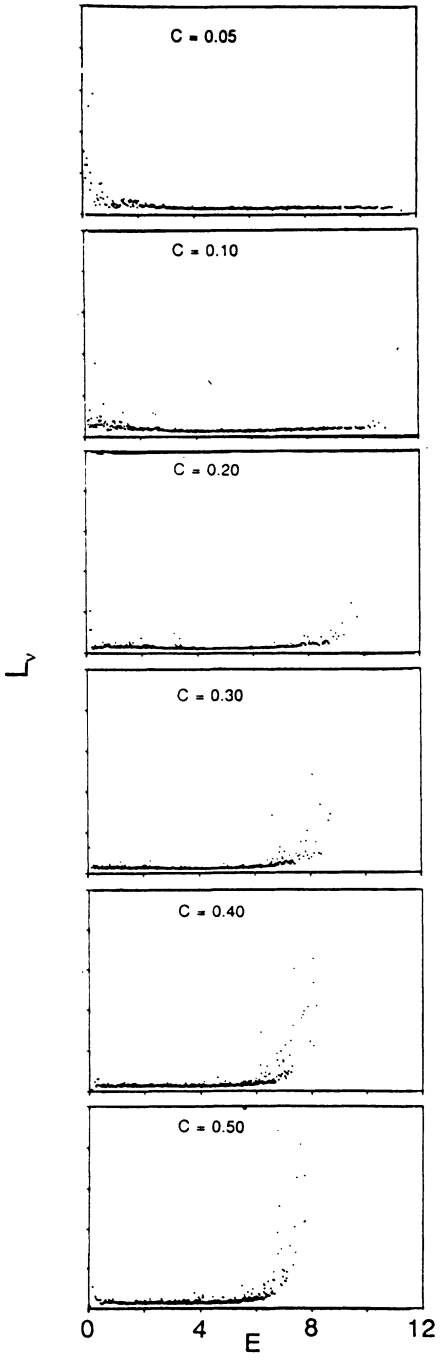

FIG. 7. Localization indices L_ν in zero field for various values of c. Other parameters the same as in Fig. 2. In all panels, the vertical scale is between 0 and 0.10.

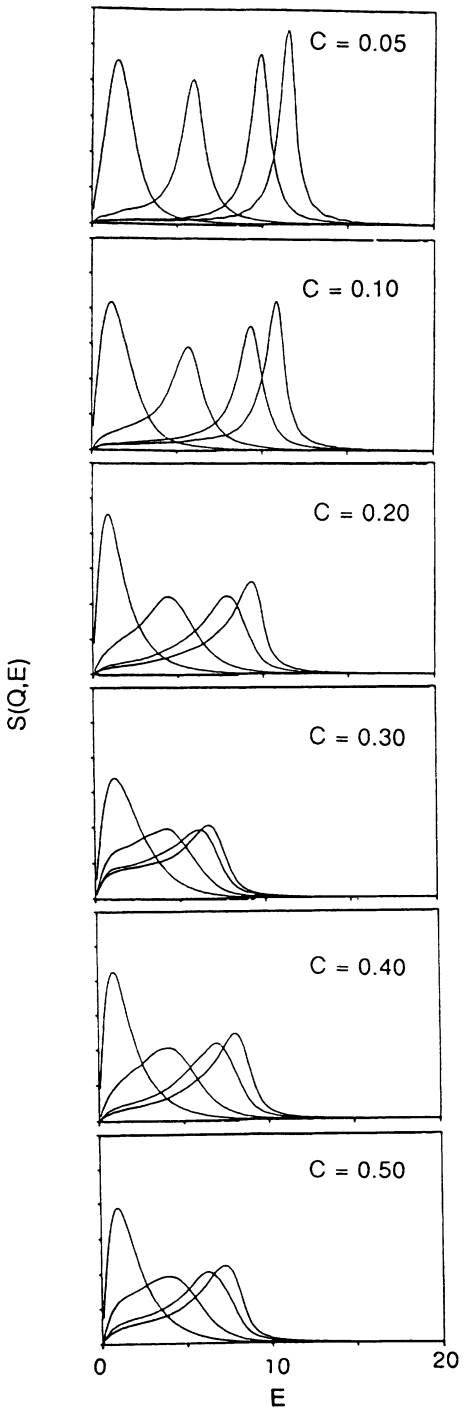

FIG. 8. Zero-temperature dynamic structure factor in zero field for various values of c. Viewed from right to left, the four curves correspond to $\mathbf{Q}=(\pi/8)(n,n,n)$ with $n=8$, 6, 4, and 2. Other parameters the same as in Fig. 3. In all panels, the vertical scale is between 0 and 0.6.

ACKNOWLEDGMENTS

One of us (DLH) would like to thank Professor E. F. Shender for stimulating his interest in this problem. Computer time on the Cray X-MP was provided by the Office of Basic Energy Sciences of the Department of Energy. Additional support was provided by the National Science Foundation.

[1]E. F. Shender, J. Phys. C **11**, L423 (1978).
[2]A. Ghazali, P. Lallemand, and H. T. Diep, Physica **134A**, 628 (1986).
[3]L. R. Walker and R. E. Walstedt, Phys. Rev. B **22**, 3816 (1980).
[4]R. Alben and M. F. Thorpe, J. Phys. C **8**, L275 (1975).
[5]M. F. Thorpe and R. Alben, J. Phys. C **9**, 2555 (1976).
[6]W. Y. Ching, D. L. Huber, and K. M. Leung, Phys. Rev. B **21**, 3708 (1980).
[7]R. A. Tahir-Kheli, Phys. Rev. B **6**, 2808; **6**, 2826 (1972).
[8]J. Hubbard, Proc. R. Soc. London Ser. A **281**, 401 (1964).
[9]W. Y. Ching and D. L. Huber, Phys. Rev. B **42**, 493 (1990).